Journal for ImmunoTherapy of Cancer

Chordoma recruits and polarizes tumor-associated macrophages via secreting CCL5 to promote malignant progression

Jiuhui Xu,[1,2] Qianyu Shi,[1,2] Jingbing Lou,[2] Boyang Wang,[1,2] Wei Wang,[1,2] Jianfang Niu,[1,2] Lei Guo,[1,2] Chenglong Chen,[2,3] Yiyang Yu,[1,2] Yi Huang,[1,2] Wei Guo,[1,2] Jianqiang Lan,[4] Yu Zhu,[4] Tingting Ren,[1,2] Xiaodong Tang [1,2]

To cite: Xu J, Shi Q, Lou J, *et al*. Chordoma recruits and polarizes tumor-associated macrophages via secreting CCL5 to promote malignant progression. *Journal for ImmunoTherapy of Cancer* 2023;**11**:e006808. doi:10.1136/jitc-2023-006808

► Additional supplemental material is published online only. To view, please visit the journal online (http://dx.doi.org/10.1136/jitc-2023-006808).

Accepted 27 March 2023

[1]Department of Musculoskeletal Tumor, Peking University People's Hospital, Beijing, China
[2]Beijing Key Laboratory of Musculoskeletal Tumor, Beijing, China
[3]Beijing Jishuitan Hospital, Beijing, Beijing, China
[4]Accurate International Biotechnology Co Ltd, Guangzhou, Hong Kong, China

Correspondence to
Dr Xiaodong Tang;
tangxiaodong@pkuph.edu.cn

Dr Tingting Ren;
tumorcenter@163.com

ABSTRACT

Background Chordoma is an extremely rare, locally aggressive malignant bone tumor originating from undifferentiated embryonic remnants. There are no effective therapeutic strategies for chordoma. Herein, we aimed to explore cellular interactions within the chordoma immune microenvironment and provide new therapeutic targets.

Methods Spectrum flow cytometry and multiplex immunofluorescence (IF) staining were used to investigate the immune microenvironment of chordoma. Cell Counting Kit-8, Edu, clone formation, Transwell, and healing assays were used to validate tumor functions. Flow cytometry and Transwell assays were used to analyze macrophage phenotype and chemotaxis alterations. Immunohistochemistry, IF, western blot, PCR, and ELISA assays were used to analyze molecular expression. An organoid model and a xenograft mouse model were constructed to investigate the efficacy of maraviroc (MVC).

Results The chordoma immune microenvironment landscape was characterized, and we observed that chordoma exhibits a typical immune exclusion phenotype. However, macrophages infiltrating the tumor zone were also noted. Through functional assays, we demonstrated that chordoma-secreted CCL5 significantly promoted malignancy progression, macrophage recruitment, and M2 polarization. In turn, M2 macrophages markedly enhanced the proliferation, invasion, and migration viability of chordoma. CCL5 knockdown and MVC (CCL5/CCR5 inhibitor) treatment both significantly inhibited chordoma malignant progression and M2 macrophage polarization. We established chordoma patient-derived organoids, wherein MVC exhibited antitumor effects, especially in patient 4, with robust killing effect. MVC inhibits chordoma growth and lung metastasis in vivo.

Conclusions Our study implicates that the CCL5–CCR5 axis plays an important role in the malignant progression of chordoma and the regulation of macrophages, and that the CCL5–CCR5 axis is a potential therapeutic target in chordoma.

WHAT IS ALREADY KNOWN ON THIS TOPIC

⇒ At present, the research on the immune microenvironment of chordoma is only at the initial stage, and there is no research on the mechanism of chordoma-immune cellular communications.

WHAT THIS STUDY ADDS

⇒ We revealed the immune infiltration and spatial distribution characteristics of chordoma and found that the CCL5–CCR5 axis plays an important role in the interaction of chordoma and macrophage.

HOW THIS STUDY MIGHT AFFECT RESEARCH, PRACTICE OR POLICY

⇒ The CCL5–CCR5 axis may be a target for chordoma treatment.

INTRODUCTION

Chordoma is an extremely rare and locally aggressive malignant bone tumor of mesenchymal tissue, with an incidence of only 0.8 per million people.[1] Studies suggest that chordoma originates from undifferentiated embryonic notochord remnants and occurs in the mid-axis bones, with the sacrum accounting for approximately 50% of the cases, followed by the skull base slope and the spine, accounting for 35% and 15%, respectively.[2] Chordoma is characterized by a high local relapse rate (43%–85%).[1] The clinical management of chordoma is extremely difficult, with overall survival rates of only 78% and 54% at 5 and 10 years.[3] Chemotherapy is ineffective against chordoma; radiotherapy and targeted therapy are both insensitive, with total en bloc resection being the mainstay treatment.[4] According to the latest NCCN Clinical Practice Guidelines in Oncology V.2.2023 (https://nccn.medlive.cn/), only recurrent chordoma was treated with systemic therapy; further, there was no preferred intervention for chordoma therapy. Thus, the development of novel drugs against chordoma is an urgent manner.

Tumor cells do not exist independently but together with the surrounding abundant mesenchymal cells and molecular components. Nowadays, the roles of tumor immune

microenvironment (TIME) in tumor progression are gradually revealed. TIME can enhance the malignant ability of tumor cells, promoting immune escape and regulating extracellular matrix (ECM) components; thus, various treatment targets were found in a variety of tumors. Tumor-associated macrophage (TAM) is the most abundant cell type in TIME, is highly plastic, and is divided into two subpopulations: M1 and M2 macrophage. M2 macrophage has been shown to be associated with poor prognosis in various of tumors such as colorectal and bladder cancers. Targeting TAMs has been reported as a promising strategy for cancer treatment, yet the chordoma TIME and its interactions with tumor cells remain elusive, which greatly hinder the development of targeted therapies and immunotherapy.

In the present study, we first characterized the chordoma microenvironment, showing macrophage infiltration into the tumor parenchyma. Further, we demonstrate that chordoma accelerated tumor progression through autocrine CCL5 acting on tumor cells and paracrine CCL5 polarizing macrophages into M2 TAMs to facilitate immune escape. Targeting M2 macrophages and the CCL5–CCR5 axis is therefore expected to improve the prognosis of patients with chordoma.

METHODS

Cell culture and coculture system

The chordoma cell line MUG-Chor1 and the human monocyte cell line THP-1 were purchased from the American Type Culture Collection. The rat tail type I collagen (354236, BD Biosciences) was added to the culture flask and incubated at room temperature for 1 hour before the MUG cells were added. MUG cells were cultured in Iscove's modified Dulbecco's medium (HyClone) and RPMI-1640 medium (Gibco) (4:1), with 12% fetal bovine serum (FBS, Wisent), 1% penicillin–streptomycin (PS, Gibco), and 1% L-glutamine (25030081, Gibco). THP-1 cells were cultured in RPMI-1640, supplemented with 10% FBS and 1% PS. All cells were cultured in an incubator at 37°C in humidified air with 5% CO_2 and stored in CELLSAVING solution (New Cell & Molecular Biotech) at −80°C.

For the coculture system, a 0.4 µm pore-size Transwell apparatus (14112, LabSelect) was used, with 5×10^5 macrophages or 5×10^5 MUG cells cultured in the bottom or top chamber based on experimental requirements.

Macrophage induction

A total of 5×10^5 THP-1 cells were seeded into a six-well plate, and 150 nM phorbol-12myristate-13-acetate (HY-18739, MCE) was added for 24 hours to induce THP-1-derived macrophages (THP-1-DMs). Monocytes were isolated from peripheral blood mononuclear cells (PBMCs) of a healthy donor and cultured in a six-well plate, where 20 ng/mL macrophage colony-stimulating factor (M-CSF) (96-AF-300-25-10, PeproTech) was added. After 3 days, half the volume of the medium was replaced, with 10 ng/mL M-CSF added for another 2 days. We then obtained the monocyte-derived macrophages (MDMs). Subsequently, the macrophages were polarized into M2 macrophages through induction with 20 ng/mL interleukin (IL)-4 (200–04, Peprotech) and 20 ng/mL IL-13 (200–13, Peprotech) for 48 hours. Cell morphology was observed under a microscope (Leica), and M2 polarization was confirmed based on marker CD206 using flow cytometry.

MACROPHAGE

Multiplex immunofluorescence (mIF) staining

mIF was performed using the PANO 7-plex immunohistochemistry (IHC) kit (10004100100; Panovue, Beijing, China) according to the manufacturer's protocol. Slides were deparaffinized at 65°C in the oven overnight, rehydrated using xylene and ethanol, followed by antigen retrieval via microwave treatment. Primary antibodies (panel 1: CD3/CD8A/CD20/PD-L1/CD56, panel 2: CD68\CD163\CD206\IRF8) (online supplemental table 1) were sequentially applied, followed by Horseradish Peroxidase (HRP)-conjugated secondary antibody incubation and tyramide signal amplification. Prior to the subsequent primary antibody incubation, the slides were microwaved to strip antibodies from the previous staining round. Nuclei were stained with 4′-6′-diamidino-2-phenylindole (DAPI) (Sigma-Aldrich). The stained slides were scanned using the Mantra System (PerkinElmer, Waltham, Massachusetts, USA) to obtain multispectral images.

Spectrum flow cytometry

Five fresh sterile chordoma tissues were obtained from the Peking University People's Hospital. Tissues were mechanically disaggregated into 3–4 mm^3 samples and digested with Collagenase IV (C8160, Solarbio) and Dispase II (D6430, Solarbio) at 37°C, with agitation on a Thermo-Shaker (MSC-100) for 30 min to generate single-cell suspensions. The dissociated tissues were filtered using Cell Strainer (431750, Falcon). Live cells were transferred into the flow tube, and 5 µL of FcX was added, followed by incubation for 10 min at room temperature in the dark. A surface staining antibody mixture (online supplemental table 2) was added and mixed well, followed by incubation for 25 min at room temperature in the dark. Thereafter, we added 2 mL of washing solution, centrifuged, discarded the supernatant, and added 1 mL of dye to identify dead and viable cells, incubating at room temperature for 10 min. The cell mass was washed three times; samples were tested on the Aurora spectral flow cytometer (Cytek). Data analysis was performed using the SpectroFlo V.3.0.0 (Cytek) software. The OMIQ platform (https://www.omiq.ai/) was used for subsequent processing of dimensionality reduction analysis results.

Cell Counting Kit-8 (CCK8), colony formation, and Edu assays

MUG cells were seeded at a density of 5×10^3 cells/well. The cells were then subjected to different treatment

conditions. After 48 hours of incubation, 10 µL CCK8 reagent (Dojindo) was added to 100 µL culture medium, following the manufacturer's instructions. The cells were incubated for 2 hours in an incubator, and the optical density at 450 nm was measured using a microplate reader (Bio-Rad).

The cells were seeded at a concentration of 8000 cells/well, incubated overnight, and received different treatments. The culture medium was changed every 3 days. After 20 days of culturing, the cells were fixed with 4% fixative solution (P1110, Solarbio) and stained with 0.1% crystal violet stain solution (G1063, Solarbio) for observation.

Edu assays were performed using BeyoClick Edu cell proliferation kit with Alexa Fluor 555 (C0075S, Beyotime Biotechnology). All groups of cells were cultured in 50 µmol/L Edu solution for 2 hours at 37°C before staining. Stained cells were photographed using a fluorescence microscope.

Apoptosis analysis via flow cytometry

The cells were stained with the fluorescein isothiocyanate (FITC) annexin V apoptosis detection kit I (556547,BD Biosciences) as per the manufacturer's instructions and examined on a flow cytometer (C6 Plus, BD Biosciences).

Cells were washed twice with phosphate-buffered saline (PBS) and subsequently stained with antibodies against CD206 (321109, BioLegend) or CD163 (333605, BioLegend) in PBS with 0.1% BSA for 30 min at 4°C. Cells were then collected for examination via flow cytometry. FlowJo V.10 (BD Biosciences) software was used for the analysis.

RNA isolation and quantitative real-time (qRT)-PCR

Chordoma tissue was collected and ground using tissue grinding machines (KZ-III-F, Servicebio). Total RNA was isolated from cells or tissues using TRIzol reagent (15596018, Invitrogen) following the manufacturer's protocol. Complementary DNA was synthesized using PrimeScript RT Master Mix (TaKaRa Biotechnology). qRT-PCR was performed to measure target gene expression relative to that of GAPDH, using SYBR Green premix Ex Taq (RR420A, TaKaRa Biotechnology). Expression data were normalized to those of the controls, and relative expression was determined via the comparative CT method. The primer sequences are listed in online supplemental table 3.

Protein extraction and western blotting

Total protein was extracted from cell lysates using cell lysis buffer (Cell Signaling Technology). Protein concentration was measured using the BCA protein assay kit (Solarbio). Equal amounts of protein were loaded into sodium dodecyl sulfate-polyacrylamide gel electrophoresis (SDS-PAGE) gels and transferred onto polyvinylidene fluoride membranes, followed by blocking with rapid closure solution (WB1601, Biotides) for 20 min. The membranes were incubated with specific primary antibodies, including anti-vimentin (77888–1-Ig, Proteintech), anti-N-cadherin (13116, Cell Signaling Technology), anti-E-cadherin (14472, Cell Signaling Technology), anti-MMP2 (66366–1-Ig, Proteintech), anti-signal-regulatory protein α (SIRPα) (13379, Cell Signaling Technology), and anti-GAPDH (60004–1-Ig, Proteintech), at 4°C overnight. The next day, membranes were incubated with appropriate secondary antibodies at 37°C for 1 hour. Protein bands were visualized using the Image Lab Software (Bio-Rad).

Wound healing and Transwell assays

Wound healing and Transwell assays were used to evaluate cell motility. MUG cells were plated into a six-well plate and incubated at 37°C until 90% confluence. A sterile 200 µL pipette tip was used to scratch a line through the monolayer. Images of these lines were obtained at 0 hour and 4 days under the microscope, and the cell migration rate was measured using ImageJ software.

Cell migration and invasion were assessed using Transwell inserts (3422; Corning, New York, USA). The bottom chamber contained 700 µL of complete medium. A total of 5×10^4 MUG cells or macrophage cells were seeded into the upper chamber and incubated with or without maraviroc (MVC) for 3 days. Migrating cells on the underside of inserts were fixed with 4% fixative solution and stained with 0.1% crystal violet for 15 min. Stained cells remaining on the upper chamber membrane were removed gently with cotton swabs. Images were acquired using a microscope, and the number of invasive cells was measured using Image J software.

Luminex and ELISA

Quantification of 48 secreted cytokines in the single-culture system and coculture system was performed using LBX-MultiDTX-48–1 (64432836, Bio-Rad). Assays were performed as per manufacturer instructions, then read and analyzed using Luminex X-200 (Luminex).

To detect cytokine concentration, condition medium was collected and used immediately or stored at −80°C. CCL5, IL-6, and IL-8 levels were determined using ELISA kits (EK1129, EK106/2, EK108; Multisciences) as per the manufacturer's instructions. Each experiment was repeated three times to assess the consistency of the results.

siRNA transfection

siRNA against CCL5 were designed and synthesized by Tsingke Biological Technology (Beijing, China), with the sequences listed in online supplemental table 4. MUG cells were seeded in the six-well plate and incubated at 37°C until 80% confluence. Lipofectamine 3000 transfection reagent (L3000015, Thermo Scientific) was used to enhance transfection efficiency. qRT-PCR and ELISA were used to determine knockdown efficiency.

Clinical tissue specimens and tissue microarray

Fresh sterile tissues were collected in tissue preservation solution for spectrum flow cytometry assay and organoid construction, either frozen in liquid nitrogen immediately to prevent RNA degradation or fixed in 4% paraformaldehyde, embedded in paraffin, and processed into tissue arrays for subsequent immunofluorescence (IF) and immunohistochemistry assays.

H&E staining, IF, and IHC

For IF staining, cells were seeded in 48-well plates overnight and then fixed in 4% fixative solution for 15 min. Cells were washed twice with PBS and permeabilized using immunostaining permeabilization buffer with saponin (P0095, Beyotime) for 15 min. After blocking with goat serum, cells were incubated with primary antibodies against CD68 (Ab125212, Abcam) and CCR5 (Ab110103, Abcam) at 4°C overnight. On the next day, cells were washed with PBS and incubated with a CoraLite488-conjugated or CoraLite594-conjugated secondary antibody in a wet box at 37°C for 1 hour. 4′-6′-Diamidino-2-phenylindole was used to stain the nucleus. Images were obtained using a fluorescence microscope.

For IHC, tissue sections and tissue microarrays were dewaxed and incubated with primary antibodies against CCR5 and CCL5 (12000–1-AP, Proteintech) at 4°C overnight.

Organoid construction, culture, and treatment

Fresh sterile surgically resected chordoma tissues were placed into 15 mL tubes containing tissue preservation solution (Accurate Int., Guangzhou) at 4°C and transferred to the laboratory for further treatment. Tissues were washed and minced with Hanks' Balanced Salt Solution supplemented with 1% PS and 10 µM Y-27632. Cells were washed and centrifuged after dissociation from tissue using the tissue pre-treatment kit (Accurate Int., Guangzhou). The cell pellet was resuspended in advanced Dulbecco's modified Eagle medium (DMEM)/F12 and mixed with growth-factor reduced Matrigel at a ratio of 1.0:1.5. The mixtures were then distributed at a volume of 30 µL to form a half-dome and gelled at 37°C for 15 min. The organoids were cultured with advanced DMEM/F12, 1× GlutaMax, 1× B27, 10 mM nicotinaminde, 1.25 mM N-acetyl cysteine, 20 mM 4-(2-Hydroxyethyl)piperazine-1-ethanesulfonic acid (HEPES), 10 nM gastrin, 100 ng/mL Wnt3a, 200 ng/mL noggin, 250 ng/mL R-spondin-1, 10 ng/mL FGF-10, 50 ng/mL EGF, 500 nM A83-01, and 10 µM Y-27632. Depending on the outgrowth of organoids, the medium was refreshed every 2–4 days, and organoids were split at a ratio of 1:1.5–1:3.

Chordoma organoids were enzymatically digested into small clusters containing three to five single cells using TripLE and were added into each well of a 384-well plate at 2000 cells/well. After 2–3 days of recovery, organoids were treated with drugs at various concentrations for 96 hours. The maximal concentrations of drugs were 24 µM for imatinib, 32 µM for anlotinib, 24 µM for apatinib, 100 µM for MVC, and 1 µg/mL for anti-CCL5. Cell viability was then assessed using CellTiter-Glo 3D. IC_{50} values were calculated based on cell viability and concentration using GraphPad.

Whole-exome sequencing

Whole-exome sequencing was performed by Biomarker Technologies Corporation (Beijing, China). A total of 0.6 µg genomic DNA per sample was used as the input material for DNA sample preparations. DNA sequencing libraries were generated using Agilent SureSelect Human All Exon V6 kit (Agilent Technologies, California, USA) as per the manufacturer's recommendations. Raw reads were further processed using the bioinformatic pipeline tool BMKCloud (www.biocloud.net).

Xenograft chordoma mouse model

All the BALB/c nude mice were purchased from Beijing Viltalriver. To establish the xenograft chordoma model, 3×10^6/100 µL MUG cells combined with 100 µL Matrigel (0827265, ABW Bio) were subcutaneously injected into the right side of the posterior flank of the mice and randomly divided into two groups (three mice per group): the negetive control (NC) group and the MVC treatment group. After 5-week progression, an obvious tumor mass was seen in all mice. Mice were treated with 100 mg/kg MVC (intraperitoneal) for 4 consecutive days. All mice had been euthanized after another 2 weeks, and the tumor tissues and lung were dissected. The tumors were washed with PBS then photographed and weighed, and the volume was evaluated. The lungs were washed with PBS then stored in 4% paraformaldehyde for H&E staining.

Statistical analysis

Data are expressed as the mean±SD. Unpaired two-tailed Student's t-test was used for the analysis of two samples. χ^2 test was used to evaluate the difference among different groups. All statistical analyses were performed with GraphPad Prism V.9.0. The level of significance was set at a p value of <0.05.

Data availability

Data were generated by the authors and available on request.

RESULTS

M2 macrophages were the most abundant tumor-infiltrating immunosuppressive cell type

Given the rarity of chordoma, little is known regarding its TIME. To comprehensively characterize the chordoma TIME, we collected five fresh chordoma specimens and prepared single-cell suspensions immediately after surgical resection. We employed a spectral flow cytometry panel composed of 19 markers that can identify 30 unique immune cell types and functional subpopulations[5–7] (figure 1A). The gating strategy is depicted in online supplemental figure 1A. T cells were the most prominent

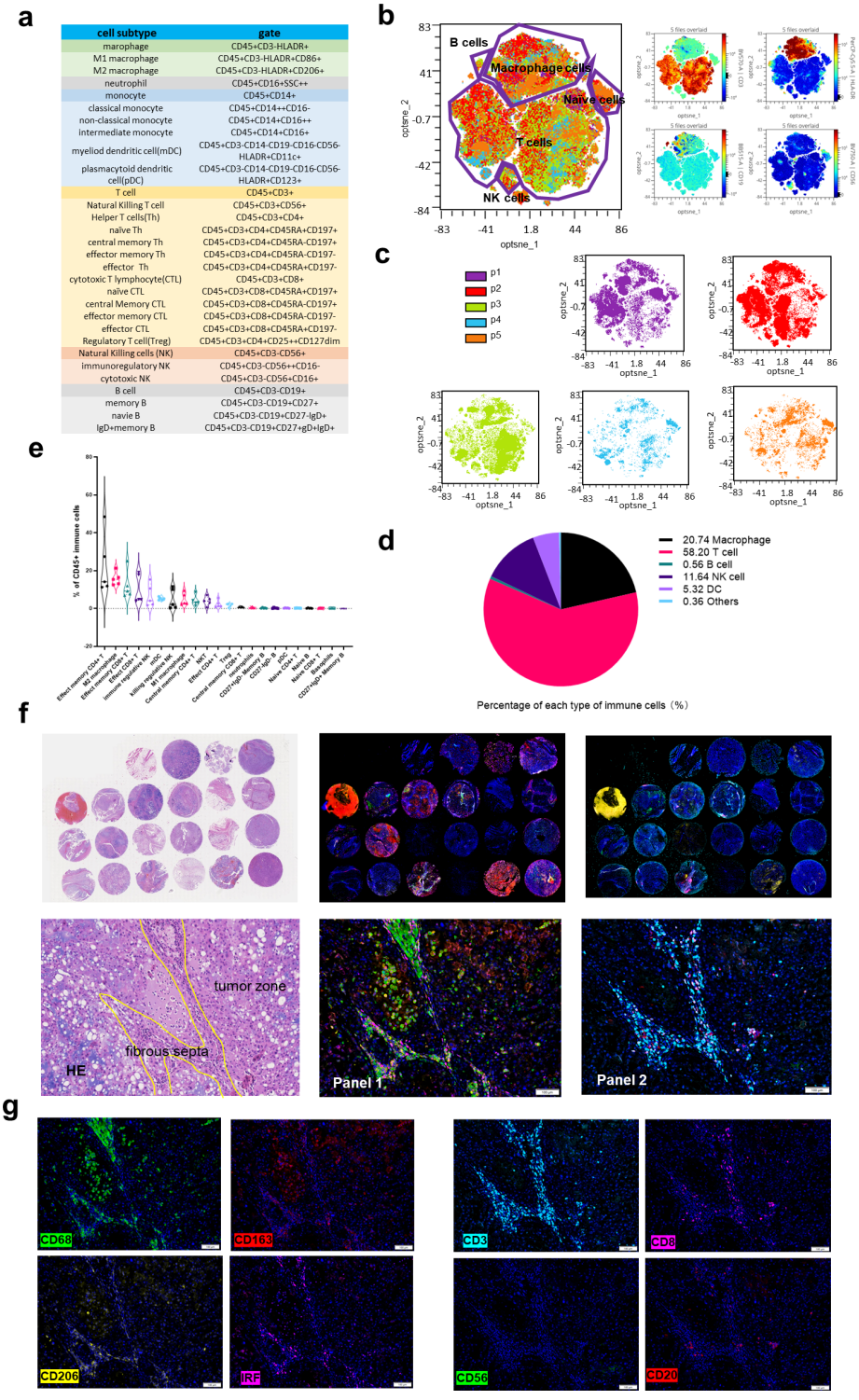

cell subtype	gate
marophage	CD45+CD3-HLADR+
M1 macrophage	CD45+CD3-HLADR+CD86+
M2 macrophage	CD45+CD3-HLADR+CD206+
neutrophil	CD45+CD16+SSC++
monocyte	CD45+CD14+
classical monocyte	CD45+CD14++CD16-
non-classical monocyte	CD45+CD14+CD16++
intermediate monocyte	CD45+CD14+CD16+
myeliod dendritic cell(mDC)	CD45+CD3-CD14-CD19-CD16-CD56-HLADR+CD11c+
plasmacytoid dendritic cell(pDC)	CD45+CD3-CD14-CD19-CD16-CD56-HLADR+CD123+
T cell	CD45+CD3+
Natural Killing T cell	CD45+CD3+CD56+
Helper T cells(Th)	CD45+CD3+CD4+
naïve Th	CD45+CD3+CD4+CD45RA+CD197+
central memory Th	CD45+CD3+CD4+CD45RA-CD197+
effector memory Th	CD45+CD3+CD4+CD45RA-CD197-
effector Th	CD45+CD3+CD4+CD45RA+CD197-
cytotoxic T lymphocyte(CTL)	CD45+CD3+CD8+
naïve CTL	CD45+CD3+CD8+CD45RA+CD197+
central Memory CTL	CD45+CD3+CD8+CD45RA-CD197+
effector memory CTL	CD45+CD3+CD8+CD45RA-CD197-
effector CTL	CD45+CD3+CD8+CD45RA+CD197-
Regulatory T cell(Treg)	CD45+CD3+CD4+CD25++CD127dim
Natural Killing cells (NK)	CD45+CD3-CD56+
immunoregulatory NK	CD45+CD3-CD56++CD16-
cytotoxic NK	CD45+CD3-CD56+CD16+
B cell	CD45+CD3-CD19+
memory B	CD45+CD3-CD19+CD27+
navie B	CD45+CD3-CD19+CD27-IgD+
IgD+memory B	CD45+CD3-CD19+CD27+IgD+IgD+

Figure 1 Depict the immune microenvironment atlas of chordoma using spectral flowcytometry and multiplex IF. (A) Markers used to gate the different populations of immune cells. (B) Opt-SNE(a dimensionality reduction analysis method) displays different immune cell clusters and expressions of major markers on the opt-SNE map. (C) The results of opt-SNE dimensionality reduction analysis showed immune infiltration phenotype in five patients. (D) Circle diagram showing the major infiltrating immune cell and its proportion in chordoma. (E) Violin chart showed the 22 immune cell subpopulation proportion. (F) H&E staining and two staining panels were performed for the infiltration of T cells, B cells, NK cells, macrophage cells, and the expression of PD-L1 in 22 chordoma tissue microarrays. A large number of immune cells were infiltrated in the fibrous septa of the chordoma. (G) Representative IF images showing different tumor-infiltrating immune cells in chordoma tissuse. Panel 1: pan macrophage (CD68-positive, green), M2 macrophage (CD163-positive, red), M2 macrophage (CD206-positive, yellow), and M1 macrophage (IRF-positive, pink). Panel 2: T cell (CD3-positive, blue), cytotoxic T cell (CD8-positive, pink), NK cell (CD56-positive, green), B cell (CD20-positive, red), and PD-L1 (yellow). DC, dendritic cell; IF, immunofluorescence; mDC, myeloid dendritic cell; NK, natural killer; IRF,interferon regulatory factor.

tumor-infiltrating immune cell type in chordoma, accounting for 58.20% of the total immune cells, followed by macrophages, accounting for 20.74%, followed by natural killer (NK) cells, dendritic cells, B cells, and granulocytes (figure 1B–D and online supplemental figure 2). The tumors of different patients exhibited similar immune infiltration features. For example, T cells and macrophages were the main infiltrating subtypes in all five patients, while B cells and neutrophils accounted for a minor percentage. At the same time, heterogeneity was also observed among patients, with CD4-positive T-cell infiltration being significantly greater than that of CD8-positive T cells in patient (P)2 and P3, while cytotoxic T cells represented the major infiltrating immune subpopulation in P1 and P4 (figure 1C). Further analysis of each immune cell subtype revealed that M2 macrophages (CD206-positive, 15.69%) were significantly more abundant than their M1 counterparts (CD86-positive, 4.84%), thus constituting the most prominent tumor-infiltrating immunosuppressive subtype (figure 1E).

We performed mIF staining to comprehensively characterize immune cell infiltration and spatial distribution within the chordoma TIME. Using two staining panels (panel 1: CD68\CD163\CD206\IRF8, panel 2: CD3\CD8A\CD20\PD-L1\CD56), we analyzed the infiltration of T cells, B cells, NK cells, and macrophages as well as the expression of the immune checkpoint programmed cell death ligand 1 (PD-L1), a marker of T-cell exhaustion, in 22 chordoma tissues. The chordoma TIME exhibited a characteristic immune-excluded phenotype where a large number of immune cells were present in the tumor stroma but were excluded from the tumor itself (figure 1F). T cells and macrophages were the main infiltrating cell types, consistent with the spectral flow cytometry results presented previously. CD3-positive T cells were the most abundant subtype, mainly present within the fibrous septa of chordoma, with stromal cells mediating this restriction by excluding T cells from the vicinity of cancer cells.[8 9] CD68-positive macrophages were not only distributed in the fibrous septa but also recruited into the tumor zone, where they physically interacted with tumor cells (figure 1G). CD206-positive or CD163-positive M2 macrophages distributed within the tumor zone were more abundant than IRF-positive M1 macrophages. Taken together with the spectral flow cytometry results, M2 macrophage not only accounted for a large proportion of chordoma-infiltrating immune cells but also could also break the physical barrier and accumulate within the vicinity of tumor cells, suggestive of an important role of M2 macrophages in the malignant progression of chordoma.[10]

Crosstalk between chordoma and M2 macrophages accelerated tumor progression

M2 macrophages participate in the malignant progression of various tumors through the promotion of blood and lymphatic vessel formation, immunosuppression, and drug resistance.[11–13] To gain insight into the role of M2 macrophages in chordoma progression, we induced macrophages from the THP-1 cell line as well as from healthy donor-derived PBMCs, thereafter stimulating their polarization into M2 macrophages (figure 2A). The suspended monocytes became apposed after 24 hours and gradually stretched. CD206 expression was detected to verify macrophage induction efficiency, with 64.5% and 99.4% of the THP-1 and PBMCs successfully induced into M2 macrophages, respectively (figure 2B). CCK8 and Edu assay results indicated that chordoma proliferation was enhanced by either THP-1-derived or PBMC-derived M2 macrophages (figure 2C,D). Wound healing and Transwell assays revealed that M2 macrophages could significantly enhance chordoma cell migration and invasion (figure 2E–G). Western blot analysis of epithelial-to-mesenchymal transition (EMT) markers, E-cadherin, N-cadherin, and vimentin indicated that M2 macrophages promoted a decrease in E-cadherin expression, while N-cadherin and vimentin were upregulated (figure 2H).

Macrophages are subject to extensive modulation, exhibiting considerable phenotypical heterogeneity based on the stimuli received via intercellular communication.[14] In this manner, tumor cells have been shown to induce TAMs, which in turn promote tumor progression. TAMs exhibit an immunosuppressive phenotype in various tumors, including osteosarcoma, breast cancer, and colorectal cancer.[12 15 16] Using a coculture system, we explored the effect of chordoma cells on macrophages via flow cytometry, observing that the proportion of CD206-positive macrophage cells increased, which suggested that chordoma cells can promote the polarization of macrophages into M2 TAMs, which then establish an immunosuppressive microenvironment favoring chordoma progression (figure 2I).

CCL5 is the key chemokine secreted by chordoma cells implicated in tumor progression

Cytokines and chemokines play a central role in the intercellular communication that drives cancer development, metastasis, and therapeutic resistance.[17 18] To determine key mediators involved in the chordoma–macrophage interaction, 48 cytokines were examined in conditioned media of chordoma or macrophage cells as well as in the culture supernatant of coculture systems via Luminex assays. Cytokine secretion is summarized in a heatmap, with 8 upregulated and 13 downregulated cytokines in the coculture system (figure 3A and online supplemental figure 3A). In order to further investigate the key regulatory factors involved in the promotion of TAMs by chordoma, the expression of 11 cytokines involved in tumor-macrophage interactions, as per the literature,[19–22] was assessed via PCR (primers are listed in online supplemental table 3). IL-6, IL-8, CCL5, and IL-13 were all upregulated in the chordoma coculture (figure 3B and online supplemental figure 3B). Thus, IL-6, IL-8, and CCL5 were significantly elevated at both the mRNA and protein levels (figure 3C). We measured the levels of secreted IL-6, IL-8, and CCL5

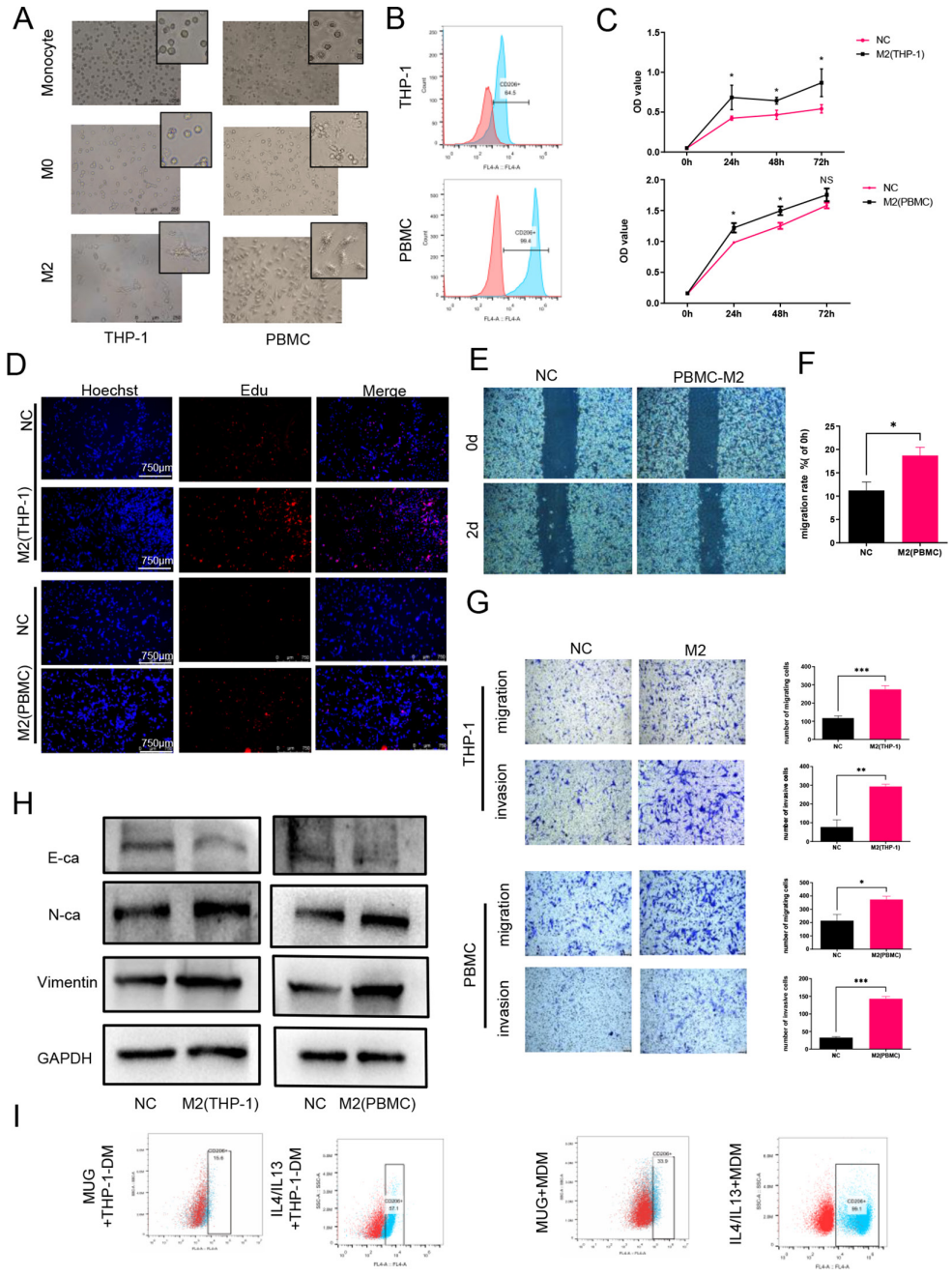

Figure 2 Intercommunication between chordoma and M2 macrophages promotes tumor progression. (A,B) Induced THP-1-derived M2 macrophage and PBMC-derived M2 macrophage were verified by microscopic photography and flow cytometry to detect CD206 expression. (C,D) CCK8 and EDU assays showed M2 macrophage enhanced chordoma proliferation viability. (E,F) The results of wound healing showed M2 macrophage accelerated chordoma migration viability. (G). THP-1 derived and PBMC-derived M2 macrophage both facilitated the migration and invasion viability of chordoma. (H). Western blot showed that M2 macrophages resulted in a decrease in epithelial protein E-cadherin and increased the expression of mesenchymal protein N-cadherin and vimentin. (I) Flow cytometry showed chordoma cells induced macrophage into M2 type (CD206-positive). CCK8, Cell Counting Kit-8, IL, interleukin; MDM, monocyte-derived macrophage; PBMC, peripheral blood mononuclear cell.

in single-cultured MUG cells, single-cultured macrophages, as well as in a coculture system via ELISA, and the results were consistent with those obtained via Luminex (online supplemental figures 4 and 5). The secretion of IL6, IL-8, and CCL5 was compared between single-cultured and cocultured MUG cells, and we found a 4.745-fold increase in CCL5 under the latter condition (figure 3D). To determine whether one cell type or both exhibited increased CCL5 secretion, the supernatants of single-cultured chordoma cells, single-cultured macrophages, cocultured chordoma cells, and cocultured macrophages were analyzed. Coculture had no impact on THP-1-DMs, with a slight increase of CCL5 secretion for MDMs. In addition, an obvious increase in CCL5 secretion by MUG cells was observed (figure 3E,F). These results indicated that CCL5 secreted by chordoma

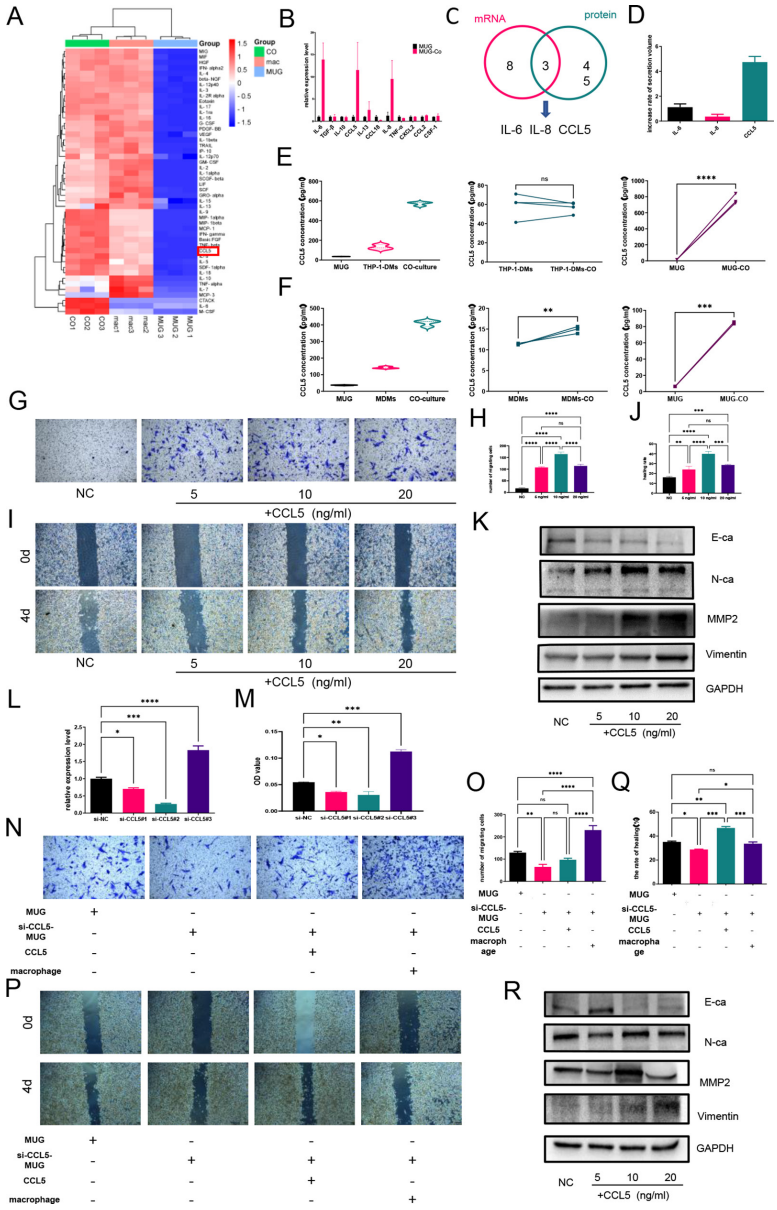

Figure 3 CCL5 secreted by chordoma was the key cytokine involved in cellular communication between chordoma cells and macrophage cells. (A) Heat-map representation of the differentially secretion in MUG, macrophage single culture systems versus MUG–macrophage coculture system. (B) Heat-map of qRT-PCR results showed the expression levels of IL-6, IL-8, CCL5, IL-1β, and IL-13 were all upregulated in cocultured MUG cells. (C) IL-6, IL-8, and CCL5 were significantly elevated in the coculture system from both RNA and secreted protein expression levels. (D) The secretion of CCL5 by MUG cells was the most drastically increased at 4.745-fold using ELISA assay. (E,F) ELISA assay results showed the secretion of CCL5 in MUG, macrophage supernatants, MUG–macrophage coculture supernatant, and cocultured MUG or macrophage supernatant. (E). Secretions of MUG and THP-1-DMs were at a low level but were obviously increased in the coculture system. Cocultured THP-1-DMs did not secrete more CCL5, but an obvious increase in CCL5 secretion by MUG cells was shown. (F) Secretions of MUG and MDMs were at a low level but were obviously increased in the coculture system. A modest increase in CCL5 secretion was seen in cocultured MDMs, and an intense increase in CCL5 secretion was shown by cocultured MUG cells. (G,H) Transwell assay showed CCL5 obviously increased chordoma cell migration viability at 5, 10, 20, and 10 ng/mL CCL5 caused the most significant functional change. (I,J) Healing wound assay showed CCL5 significantly enhanced chordoma healing at different concentrations, and 10 ng/mL CCL5 caused the most obvious functional change. (K) Western blot results indicated CCL5 induced chordoma epithelial–mesenchymal transition in a concentration-dependent effect and increased MMP2 expression. (L,M) CCL5 expression level was validated by qRT-PCR (L) and ELISA assay (M). After siRNA treatment (N,P), Transwell (N) and wound healing assays (P) showed chordoma cell migration viability was decreased by si-CCL5 transfection and reversed after adding exogenous CCL5 or coculture with macrophage. (O–Q) Statistical analysis results of Transwell and wound healing assays. (R) Western blot showed E-cadherin expression was increased, and N-ca, vimentin, and MMP2 were decreased after CCL5 reduction, and the protein expressions were inverted by adding exogenous CCL5 or coculture with macrophage. *P<0.05, **P<0.01, ***P<0.001, ****P<0.0001. IL, interleukin; MDM, monocyte-derived macrophage; ns, not significant; THP-1-DM, THP-1-derived macrophage.

cells may play a crucial role in the intercellular communication with macrophages.

CCL5 secreted by chordoma cells promoted chordoma migration and EMT

To confirm the function of CCL5 in chordoma, we administered exogenous CCL5 to chordoma cells, yet failed to elicit an effect based on wound healing assays and the levels of EMT-related proteins after 48 hours of treatment (online supplemental figure 6A,B). Considering the slow-growing nature of chordoma, we extended the duration of CCL5 treatment. Subsequent Transwell and wound healing assays indicated that CCL5 significantly promoted chordoma migration at multiple concentrations (5, 10, and 20 ng/mL), with 10 ng/mL exerting the most pronounced effect (figure 3G–J). Further, western blot results revealed that E-cadherin expression levels decreased significantly, while those of vimentin and N-cadherin increased (figure 3K), indicating that CCL5 promotes the EMT of chordoma. The expression of MMP2, which is a major ECM-degrading enzyme that facilitates tumor invasion,[23] was also increased (figure 3K). CCK8, Edu, and clone formation assays indicated no significant effect on cell proliferation at multiple CCL5 concentrations and treatment durations (online supplemental figure 7A–C).

To further examine the function of CCL5 in tumor progression, three siRNAs were designed to interfere with CCL5 expression (sequences shown in online supplemental table 4). We verified silencing efficiency via PCR and ELISA. The second si-CCL5 suppressed CCL5 expression to the greatest extent and was therefore used in subsequent experiments (figure 3L,M). Si-CCL5 MUG cells exhibited a lesser EMT, while exogenous CCL5 administration or coculture reversed this inhibition and significantly upregulated MMP2 expression (figure 3R). Transwell and wound healing assays indicated that interfering with CCL5 compromised chordoma cell migration, which was rescued on addition of exogenous CCL5 (figure 3N–Q).

CCL5 promoted polarization into M2 TAMs and upregulated SIRPα expression

Further confirming the association between CCL5 and macrophage polarization, CD206 expression in macrophages was significantly upregulated by exogenous CCL5, with an increase in the CD206-positive cell fraction from 15.0% to 32.6% following incubation with 10 ng/mL CCL5 (figure 4A). SIRPα is an immune checkpoint expressed on macrophages and a ligand of CD47, a receptor often overexpressed on cancer cells.[24] The CD47–SIRPα interaction constitutes the 'don't eat me' signal, impeding macrophage activation and phagocytosis.[25] Western blot analysis indicated that SIRPα expression was enhanced by exogenous CCL5 in a concentration-dependent manner (figure 4B). Further, a considerable increase in macrophage chemotaxis was observed (figure 4C,D).

We then assessed whether suppressing CCL5 expression in chordoma could result in macrophage repolarization. Coculturing with MUG cells induced M2 macrophage polarization and an increase in SIRPα expression levels, whereas coculturing with si-CCL5 MUG cells did not, and exogenous CCL5 slightly stimulated M2 macrophage polarization and upregulated immune checkpoint levels (figure 4E,F). After preplating MUG and si-CCL5 MUG cells, Transwell assay results indicated that chordoma cells recruited macrophages, whereas si-CCL5–MUG cells inhibited macrophage chemotaxis, which could only be rescued via addition of exogenous CCL5 (figure 4G,H).

Blocking the CCL5–CCR5 axis by MVC prevented malignant progression of chordoma in vitro

CCL5 is currently known to bind several receptors, including CCR1, CCR3, CCR4, and CCR5.[26] CCR5, a seven-transmembrane G protein-coupled receptor with the highest affinity for CCL5, is expressed on various cell types, including T cells, macrophages, and various tumor cells.[27] We decided to determine whether the effects of CCL5 observed herein are mediated via the CCL5–CCR5 axis. Robust CCR5 expression was observed on both MUG cells and macrophages via IF (figure 5A). IHC staining was performed on 48 chordoma tissues, revealing robust CCR5 expression in all samples (figure 5B). Further, CD68-positive macrophages colocalized with CCR5 (figure 5C). These results indicate that both chordoma cells and macrophages expressed CCR5.

MVC, a CCR5 antagonist, is the first Food and Drug Administration-approved drug for treating HIV infection and is now being repurposed for cancer therapy.[28] We used MVC to verify whether the CCL5–CCR5 axis mediated the chordoma–macrophage interaction and whether MVC holds potential as a therapeutic against chordoma. We determined the 48-hours IC_{50} value of MVC against MUG cells as 50.53 µM (figure 5D). Thus, 30 µM MVC was used in subsequent experiments. Blocking the CCL5–CCR5 axis via MVC inhibited chordoma migration (figure 5E–H). Further, MVC mildly suppressed the chordoma EMT as well as macrophage immune checkpoint expression (figure 5I,J). The proportion of CD206-positive cells induced by exogenous CCL5 was significantly reduced by MVC (figure 5K,L). Transwell assay results also indicated that MVC could inhibit macrophage migration by blocking the CCL5–CCR5 axis (figure 5M,N). In the chordoma mouse model, MVC treatment inhibited the chordoma growth as shown in figure 5O; however, it demonstrated a non-significant difference in tumor weight and volume when statistical analysis was performed, which we suggest may be due to the inadequate samples in each group (figure 5O–Q). Additionally, lung metastasis was seen in the NC group, which indicated MVC also could inhibit chordoma lung metastasis (figure 5R).

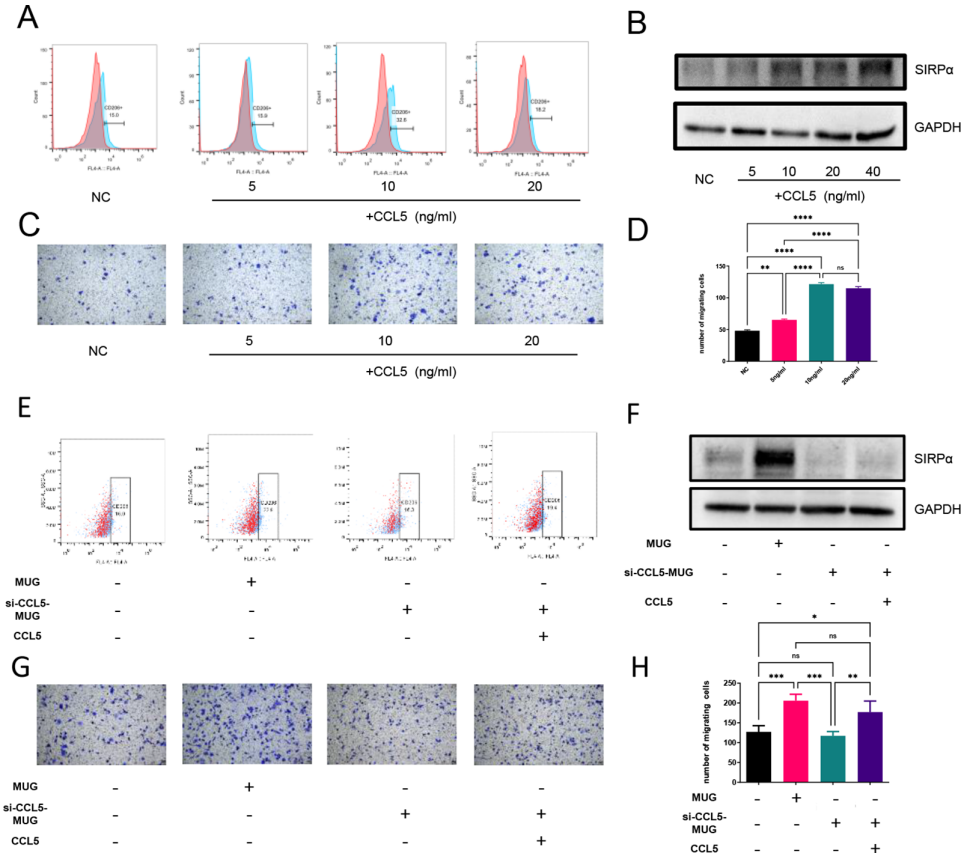

Figure 4 CCL5 educated macrophage into M2 macrophage and facilitated macrophage chemotaxis. (A) CD206 expression on macrophage surface was increased by adding CCL5 at different concentrations, and 10 ng/mL CCL5 caused the most obvious macrophage polarization, which was tested by flow cytometry. (B). Western blot showed exogenous CCL5 increased SIRPα expression on macrophage in a concentration-dependent effect . (C) Transwell assay indicated macrophage cells chemotaxis viability was increased by CCL5, and the most significant chemotaxis viability change was seen at the concentration of 10 ng/mL. (D) Statistical analysis results of macrophage chemotaxis. (E) Flow cytometry results showed that coculture with MUG cells promoted the M2 macrophage polarization, and coculture with siCCL5–MUG cells did not affect macrophage CD206 expression, which was increased by adding CCL5. (F) The results of western blot showed immune checkpoint SIRPα on marcophage was significantly increased with coculture with MUG, while with coculture with siCCL5–MUG cells, SIRPα expression was not obviously changed. Adding exogenous CCL5 into siCCL5–MUG–macrophage coculture system just lightly increased SIRPα expression. (G,H) Transwell assays results showed that preplating MUG cells promoted the macrophages chemotaxis, and preplating siCCL5–MUG cells did not affect macrophage chemotaxis, which was enhanced by exogenous CCL5. *P<0.05, **P<0.01,***P < 0.001,****P < 0.0001. ns, not significant; SIRPα, signal-regulatory protein α.

MVC exhibited antitumor effects in chordoma organoids

Patient-derived organoids (PDOs) are a promising three-dimensional cellular system widely employed within the drug development pipeline.[29 30] We successfully established organoids from five patients with chordoma, thereafter subjecting them to drug sensitivity testing (figure 6A,B). The clinical characteristics of patients with chordoma are listed in online supplemental table 5). First, to verify chordoma organoids, we compared the morphological features of parental tumor tissue and the organoid using H&E staining, with the results showing that the original chordoma features were well preserved in organoids. They all displayed round nuclei, lobules, and vacuolated (physaliferous) neoplastic cells with multiple intracytoplasmic vacuoles (figure 6C). Brachyury is a typical chordoma marker, uniquely overexpressed in almost all chordoma cells while being absent in the other mesenchymal cells within the tumor microenvironment.[31] Robust nuclear brachyury was detected in both parental tumors and organoids (figure 6D). In addition, exome sequencing was further performed; molecular features were retained in the organoids, and they matched tumor tissues. Comparative exome analysis was carried out for P2 and P4, confirming the concordance between organoids and corresponding tumor tissues (P2, 90.75% of the concordance; P4, 99.08% of the concordance). Genome-wide distributions in chromosomes were also in agreement (figure 6E). Single-nucleotide polymorphism as well as indel and copy number variation analyses further confirmed that the genetic features of chordomas were retained in our organoids (figure 6F and online supplemental file 1). Drug sensitivity testing was then performed on PDOs, with the exception of organoids from P5, which were excluded owing to an insufficient number

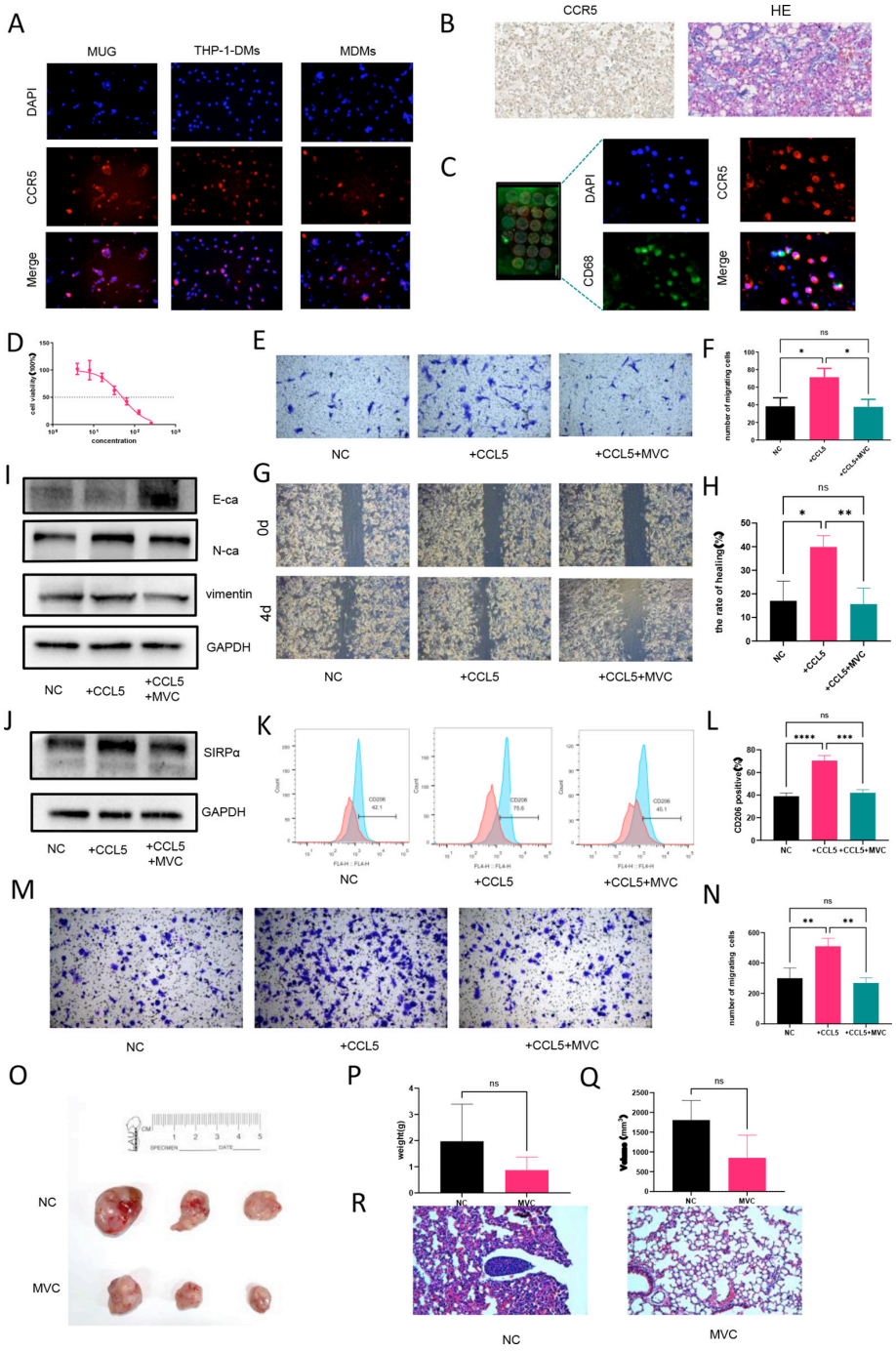

Figure 5 Treatment of MVC suppressed malignant progession of chordoma and macrophage polarization. (A) MUG, THP-1-DMs, and MDMs were stained with DAPI (blue) and CCR5 (red). (B) Chordoma tissue microarrays were assessed immunohistochemically in CCR5 expression, and the results showed CCR5 was highly expressed on chordoma cells. (C) Triple fluorescent staining with DAPI (blue), anti-CCR5 antibody (red), and anti-CD68 antibody (red) showed macrophages expressed CCR5 in chordoma microenvironment. (D) The viability of MUG cells with the treatment of MVC from the concentration of 0–128 µM. The 48-hour IC_{50} value of MUG is 50.53 µM. (E,F) Transwell assay results demonstrated that blocking the CCL5–CCR5 axis by adding MVC into the upper chamber of Transwell plates inhibited chordoma cell migration. (G,H) Wound healing assay results showed MVC reversed the increased chordoma cell healing rate caused by CCL5. (I) Western blot showed EMT-related protein E-cadherin was increased, and N-ca and vimentin expressions were decreased after MVC treatment. (J) Western blot showed MVC reduced the increased immune checkpoint SIRPα expression on macrophages induced by CCL5. (K,L). The results of flow cytometry showed MVC decreased M2 polarizated macrophages caused by CCL5. (M,N) Transwell assay results indicated MVC reversed the increased macrophage migrating viability caused by CCL5. (O) Xenograft photographs were taken after 14-day administration. (P) Results of tumor weights on the day the mice were euthanized. (Q) Results of tumor volume on the day the mice were euthanized. (R) Representative images of lungs harvested from mice. *P<0.05, **P<0.01, ***P<0.001, ****P<0.0001. EMT, epithelial-to-mesenchymal transition; MDM, monocyte-derived macrophage; MVC, maraviroc; ns, not significant; SIRPα, signal-regulatory protein α; THP-1-DM, THP-1-derived macrophage.

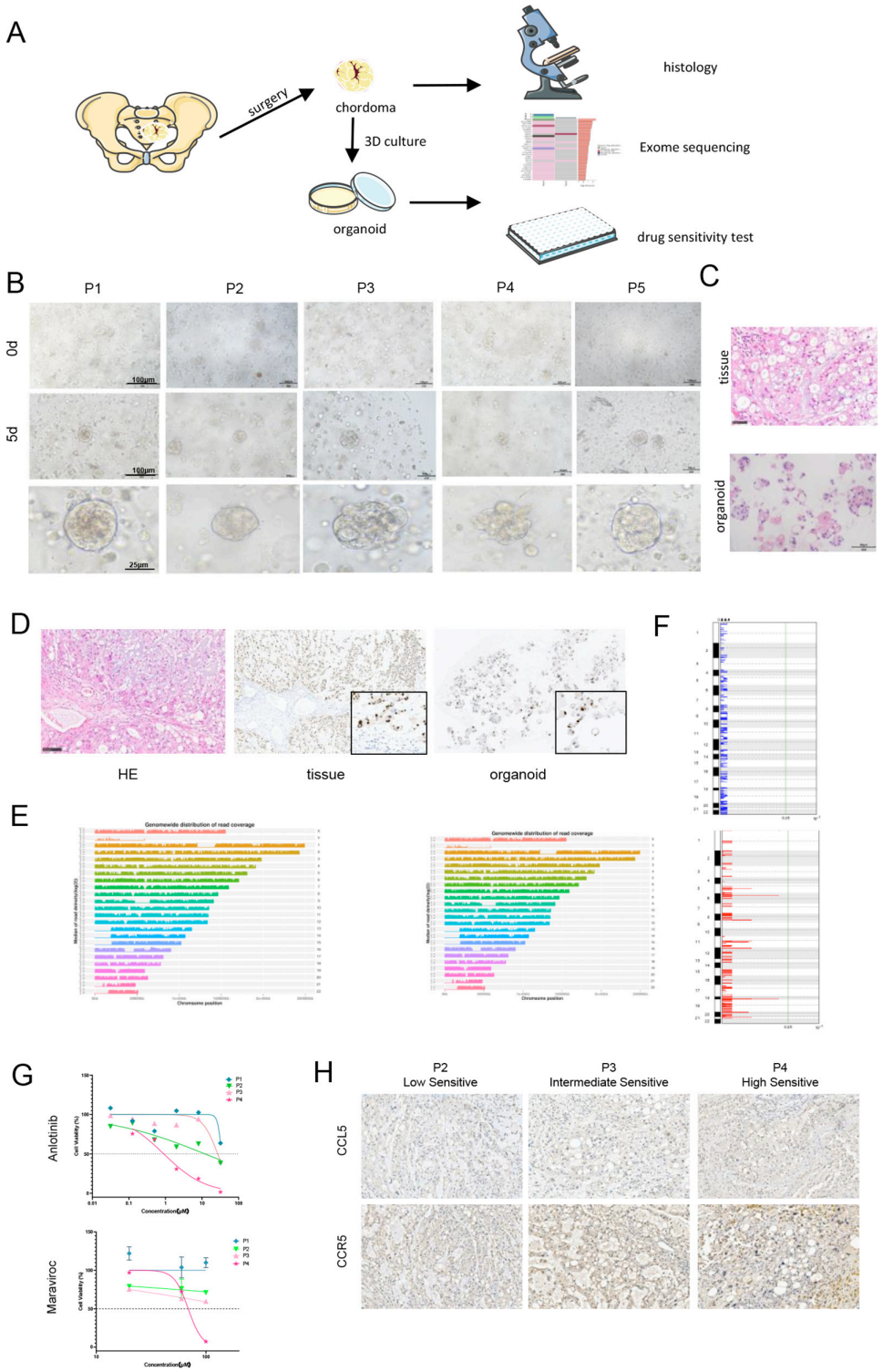

Figure 6 Blocking the CCL5–CCR5 axis inhibited tumor malignant progression in chordoma organoid. (A) Schematic illustration for chordoma organoid established, validation and drug test. (B) Chordoma organoids were visualized by brightfield in 0 day and 5 days. Scale bar, 200 μm. (C) H&E staining on both the parent tumor tissues sections and organoid showed chordoma morphological features were well conserved. (D) IHC staining showed Brachyury was highly expressed in chordoma tissues and organoids; organoids preserved features of the parent tumor. (E) Genome-wide distributions in chromosomes of parental tumor tissues and organoids. (F) CNV was compared between tumor tissues and organoids, and the results indicated no significant difference was shown. (G) The IC_{50} values of anlotinib and MVC in organoid patients. Anlotinib was used as the positive control of chordoma treatment. (H) CCL5 and CCR5 IHC staining in the parent tumor tissues. The results showed CCL5 and CCR5 expressions were correlated with sensitivity to MVC. CNV, copy number variation; IHC, immunohistochemistry; MVC, maraviroc.

Table 1 Drug sensitivity results of chordoma organoids

	P1		P2		P3		P4	
Drug	IC_{50}	MIR* (%)	IC_{50}	MIR (%)	IC_{50}	MIR (%)	IC_{50}	MIR (%)
Anlotinib	9.00	36.34	1.50	61.63	3.35	59.49	0.11	98.44
Imatinib	14.20	37.15	>20	47.76	–	–	–	–
Apatinib	>20	0.00	>20	41.21	–	–	–	–
Anti-CCL5	>5	5.52	>5	28.82	0.93	51.07	>5	2.58
Maraviroc	>500	0.00	>500	29.12	217.20	40.41	68.97	92.79

MIR, maximum concentration inhibition rate; P, patient.

of cells. The drug testing panel consisted of anlotinib, imatinib, apatinib, anti-CCL5, and MVC. Anlotinib, imatinib, and apatinib were used as positive controls for chordoma treatment.[32–34] Owing to an insufficient number of cells, P3 and P4 organoids were subjected to anlotinib as a positive control. Anti-CCL5 exhibited a moderate therapeutic effect in all four PDOs, while MVC efficacy varied among patient organoids. More specifically, 100 µM MVC exhibited no antitumor effect in P1, while low and intermediate MVC sensitivity was observed in P2-derived and P3-derived organoids, respectively. Further, MVC exhibited a robust inhibitory effect (92.79%) in the P4-derived organoid, which was comparable to the effect of anlotinib (98.44%). The IC_{50} values of anlotinib and MVC are shown in figure 6G. Imatinib, apatinib, and anti-CCL5 IC_{50} values are shown in online supplemental figure 8) (table 1). IHC analysis further revealed that CCL5/CCR5 expression was correlated with MVC antitumor efficiency in organoids (figure 6H).

CCL5 and CCR5 were highly expressed in chordoma and correlate with tumor recurrence

We demonstrated that CCL5 could promote chordoma invasion and migration, although whether CCL5 expression correlates with patient prognosis remained unclear. To address this, we collected 16 surgically resected chordoma specimens. The relationships between CCL5 mRNA expression and clinical characteristics were analyzed (figure 7A). High CCL5 expression was correlated with chordoma recurrence (figure 7B). Furthermore, we obtained 48 chordoma specimens (22 tissue microarrays and 26 tissue sections) for CCL5 and CCR5 IHC staining, with the clinical information of patients shown in online supplemental table 6. Because of debulking during the staining process and insufficient tumor samples for data analysis, 41 cases were scored for CCL5 IRS and 46 for CCR5 IRS. CCL5 and CCR5 both exhibited robust expression (figure 7C), with high CCL5 IRS (9–12) in 58.54% of the cases (figure 7D). CCR5 expression was positively correlated with CCL5 (figure 7E). Further, CCR5 expression was significantly higher in patients with recurrent chordoma, which indicates that the CCL5–CCR5 axis was associated with chordoma recurrence (figure 7F).

DISCUSSION

Chordoma is a rare tumor, for which a comprehensive landscape of the TIME is currently lacking, thus limiting the identification of novel therapeutic targets. Uncovering crosstalk within the TIME is essential for understanding tumor immune escape and electing targets of clinical significance.[35] In our study, spectral flow cytometry data and mIF results provided valuable insight into cellular components within the chordoma microenvironment as well as into the tumor immune landscape. T cells were the main tumor-infiltrating immune cell type, mostly present within the fibrous septa of chordoma, which hindered contact with tumor cells. Macrophages, especially M2 macrophages, also extensively infiltrated chordoma, accounting for up to 15.69% of the infiltrating immune cells and penetrating the physical barrier to interact with tumor cells. In literature, descriptions of immune phenotypes in chordoma are mainly based on H&E staining and immunohistochemistry, which provides limited insight.[36–39] Surprisingly, single-cell RNA-sequencing and multiplex IF techniques were applied in studies of the chordoma TIME only since last year,[40 41] with their findings supporting the current results, as macrophages were reported to significantly infiltrate the chordoma parenchyma, while T cells exhibited stromal infiltration.[41] To our knowledge, this is the first report of spectral flow cytometry analysis in chordoma, also in combination with mIF for TIME characterization. Our findings suggest that immunotherapy approaches for chordoma should target the interaction of macrophage and chordoma cells or promote T-cell infiltration into the tumor parenchyma.

To gain deeper insights into the crosstalk mechanism between chordoma cells and macrophages, cytokine secretion was screened and validated via Luminex and ELISA, respectively, with CCL5 identified as a key mediator of intercellular communication. CCL5, also known as RANTES (regulated on activation, normal T cell expressed, and secreted) has been reported to promote tumor progression by inducing ECM remodeling and migration, supporting cancer stem cell expansion, promoting DNA damage repair, metabolic reprogramming and angiogenesis in a variety of

A

		n	CCL5 expression level	P value
age(years)	> 60	5	1.504	0.4309
	≤60	11	1.096	
gender	male	7	1.375	0.5799
	female	9	1.106	
relapase	yes	8	0.7459	0.0327*
	no	8	1.701	
surrounding invasion	yes	8	0.9128	0.1864
	no	8	1.534	

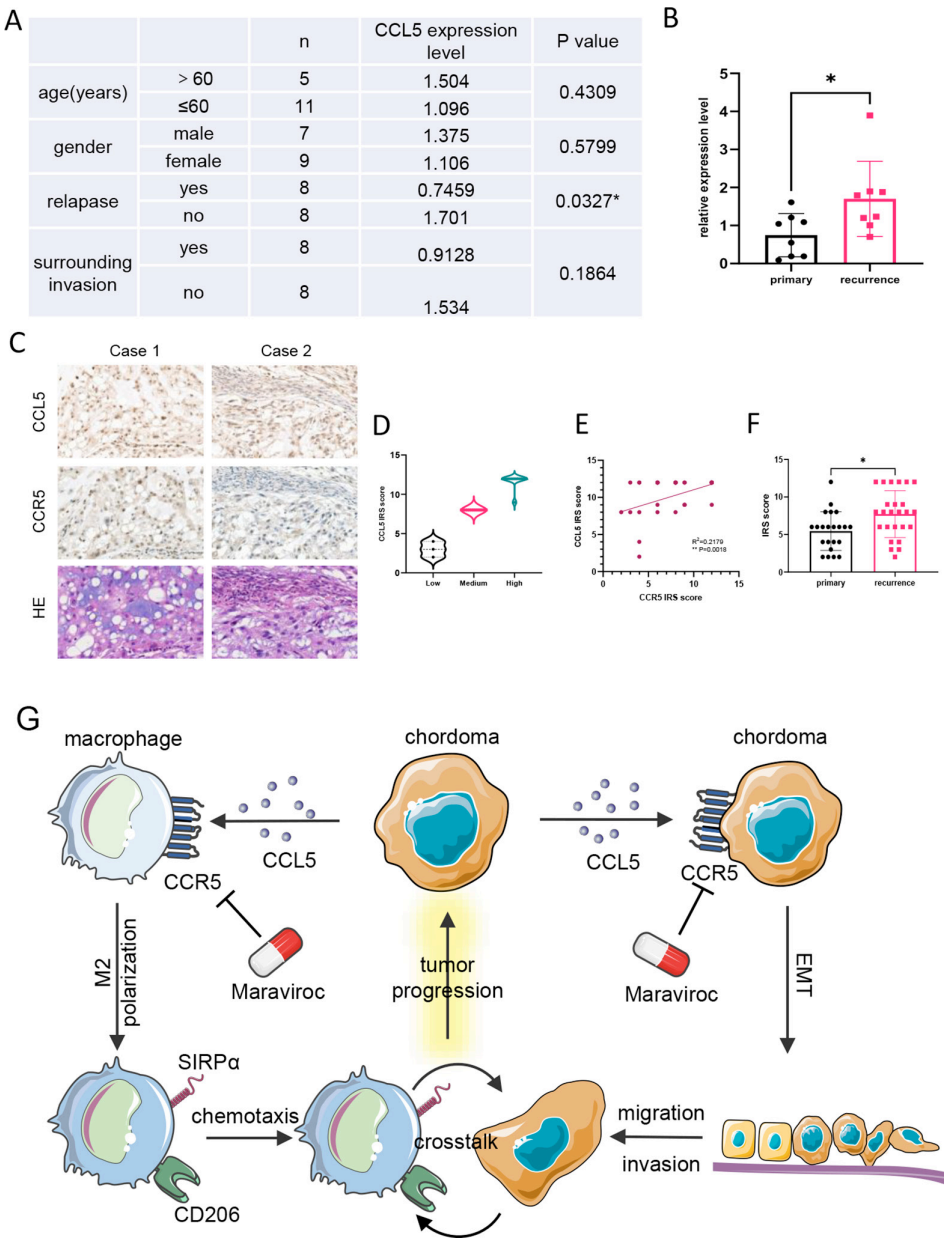

Figure 7 CCL5 and CCR5 are highly expressed and correlated with tumor recurrence. (A) The results of PCR showed CCL5 expression level was correlated with chordoma recurrence. (B) Statistical analysis of CCL5 expression in primary chordoma and recurrence chordoma tissues.(C) CCL5 and CCR5 were both shown with robust expressions in patients with chordoma. (D) CCL5 IRS score distribution in low (0–4) (n=3), medium (5–8) (n=14), and high (9–12) (n=24) classes. (E) The correlation of CCL5 expression and CCR5 expression. (F) Statistical analysis of CCLR5 expression in primary chordoma and recurrence chordoma sections. (G) Schematic diagram illustrating the hypothetical mechanisms of chordoma secreted CCL5 to recruit and polarize tumor-associated macrophages to promote chordoma malignant progression. *P<0.05, **P<0.01. EMT, epithelial-to-mesenchymal transition; SIRPα, signal-regulatory protein α.

tumors.[42–45] In our study, CCL5 secreted by chordoma cells acted on CCR5 from tumor cells to promote the EMT and enhance chordoma migration and invasion. Further, CCL5 promoted macrophage polarization into M2 TAMs, recruiting these toward the tumor parenchyma.[46] Chordoma grows slowly, yet it is a locally invasive malignancy. The postoperative local recurrence rate of chordoma is as high as 50%, even after en bloc resection. Approximately 30%–40% of the patients have metastases, typically after local recurrence.[47] Through the analysis of CCL5/CCR5 expression in clinical samples, we found that CCL5/CCR5 expression correlated with chordoma recurrence, suggesting that autocrine CCL5 promoted chordoma invasion and acted on macrophages in a paracrine manner to induce macrophage polarization and infiltration into the tumor parenchyma.

Given that chemotherapy and radiotherapy are not effective against chordoma, there is an urgent need for new therapeutic strategies. Herein, we used the CCR5

antagonist MVC to explore the effect of blocking CCL5/CCR5 signaling as a strategy against chordoma. MVC not only directly inhibited the malignant progression of chordoma in vitro and in vivo but also suppressed macrophage polarization.

Chordoma cell lines typically grow at a very slow rate, which complicates long-term culture, especially when trying to use them as preclinical models for the identification of novel anticancer therapeutics.[48] As a viable alternative, organoid culture systems recapitulate in vivo tumor cell growth,[49] dramatically accelerating the process of drug screening for slow-growing tumors, such as chordoma. We established five PDO models and observed the antitumor efficacy of MVC, which correlated with the expressions of CCL5 and CCR5, highlighting MVC as a promising drug for chordoma treatment. To our knowledge, there are only two publications on chordoma organoids,[29 30] and we have pioneered the use of chordoma organoids for target-specific drug testing. However, there are still some limitations in our study. In the mice model, we just analyzed the growth of the tumor; the immunodeficiency of nude mice limited further analysis about the macrophage phenotype and spatial characteristics, which may be further explored using a humanized mice model. In summary, we characterized the chordoma immune landscape, revealing an immune-excluded phenotype, wherein M2 macrophages were abundant within the tumor parenchyma, promoting chordoma progression. Further, CCL5 secreted by chordoma cells can drive the chordoma EMT in an autocrine manner, in addition to inducing M2 polarization and chemotaxis to the tumor area via paracrine signaling. Targeting the CCL5–CCR5 axis with MVC represents a promising treatment strategy against chordoma, as observed in vivo and PDO models (figure 7G).

Contributors XT and TR are responsible for the overall content as guarantors. TR and XT are responsible for the conception and design of the study. Acquisition, analysis and interpretation of data were performed by JX, QS, JLo, BW, YY, JLa, and YZ. The main part of the manuscript and figures were generated by JX, WW, JN, LG, CC, and YH.

Funding This work was supported by the National Natural Science Foundation of China (number 81972509) and Beijing Natural Science Foundation (7232193).

Competing interests None declared.

Patient consent for publication Not applicable.

Ethics approval This study involves human participants and was approved by ethics committee of the Peking University People's Hospital (2019PHB239-01) Participants gave informed consent to participate in the study before taking part. The animal experiment was approved by Ethics Committee of Peking university people's hospital (2019PHE054)).

Provenance and peer review Not commissioned; externally peer reviewed.

Data availability statement Data are available upon reasonable request.

ORCID iD

Xiaodong Tang http://orcid.org/0000-0003-0463-5487

REFERENCES

1 Walcott BP, Nahed BV, Mohyeldin A, *et al*. Chordoma: current concepts, management, and future directions. *Lancet Oncol* 2012;13:e69–76.
2 Bongers MER, Dea N, Ames CP, *et al*. Surgical strategies for chordoma. *Neurosurg Clin N Am* 2020;31:251–61.
3 McMaster ML, Goldstein AM, Bromley CM, *et al*. Chordoma: incidence and survival patterns in the United States, 1973-1995. *Cancer Causes and Control* 2001;12:1–11.
4 Yamada Y, Gounder M, Laufer I. Multidisciplinary management of recurrent chordomas. *Curr Treat Options Oncol* 2013;14:442–53.
5 Chevrier S, Levine JH, Zanotelli VRT, *et al*. An immune atlas of clear cell renal cell carcinoma. *Cell* 2017;169:736–49.
6 Lavin Y, Kobayashi S, Leader A, *et al*. Innate immune landscape in early lung adenocarcinoma by paired single-cell analyses. *Cell* 2017;169:750–65.
7 Stankovic B, Bjørhovde HAK, Skarshaug R, *et al*. Immune cell composition in human non-small cell lung cancer. *Front Immunol* 2018;9:3101.
8 Desbois M, Wang Y. Cancer-associated fibroblasts: key players in shaping the tumor immune microenvironment. *Immunol Rev* 2021;302:241–58.
9 Joyce JA, Fearon DT. T cell exclusion, immune privilege, and the tumor microenvironment. *Science* 2015;348:74–80.
10 Barber SM, Sadrameli SS, Lee JJ, *et al*. Chordoma-current understanding and modern treatment paradigms. *J Clin Med* 2021;10:1054.
11 Han Y, Guo W, Ren T, *et al*. Tumor-associated macrophages promote lung metastasis and induce epithelial-mesenchymal transition in osteosarcoma by activating the COX-2/STAT3 axis. *Cancer Lett* 2019;440–441:116–25.
12 Huang Q, Liang X, Ren T, *et al*. The role of tumor-associated macrophages in osteosarcoma progression-therapeutic implications. *Cell Oncol (Dordr)* 2021;44:525–39.
13 Chen C, Xie L, Ren T, *et al*. Immunotherapy for osteosarcoma: fundamental mechanism, rationale, and recent breakthroughs. *Cancer Lett* 2021;500:1–10.
14 Wang X, Tokheim C, Gu SS, *et al*. In vivo CRISPR screens identify the E3 ligase COP1 as a modulator of macrophage infiltration and cancer immunotherapy target. *Cell* 2021;184:5357–74.
15 Cassetta L, Fragkogianni S, Sims AH, *et al*. Human tumor-associated macrophage and monocyte transcriptional landscapes reveal cancer-specific reprogramming, biomarkers, and therapeutic targets. *Cancer Cell* 2019;35:588–602.
16 Yang C, Wei C, Wang S, *et al*. Elevated CD163(+)/CD68(+) ratio at tumor invasive front is closely associated with aggressive phenotype and poor prognosis in colorectal cancer. *Int J Biol Sci* 2019;15:984–98.
17 Wen Y, Zhu Y, Zhang C, *et al*. Chronic inflammation, cancer development and immunotherapy. *Front Pharmacol* 2022;13:1040163.
18 Shintani Y, Fujiwara A, Kimura T, *et al*. IL-6 secreted from cancer-associated fibroblasts mediates chemoresistance in NSCLC by increasing epithelial-mesenchymal transition signaling. *J Thorac Oncol* 2016;11:1482–92.
19 Bayik D, Lathia JD. Cancer stem cell-immune cell crosstalk in tumour progression. *Nat Rev Cancer* 2021;21:526–36.
20 Nie Y, Chen J, Huang D, *et al*. Tumor-associated macrophages promote malignant progression of breast phyllodes tumors by inducing myofibroblast differentiation. *Cancer Res* 2017;77:3605–18.
21 Anderson NR, Minutolo NG, Gill S, *et al*. Macrophage-based approaches for cancer immunotherapy. *Cancer Res* 2021;81:1201–8.
22 Lin Y, Xu J, Lan H. Tumor-associated macrophages in tumor metastasis: biological roles and clinical therapeutic applications. *J Hematol Oncol* 2019;12:76.

23 Li M, Wang Y, Li M, *et al*. Integrins as attractive targets for cancer therapeutics. *Acta Pharm Sin B* 2021;11:2726–37.
24 Veillette A, Chen J. SIRPα-CD47 immune checkpoint blockade in anticancer therapy. *Trends Immunol* 2018;39:173–84.
25 Matlung HL, Szilagyi K, Barclay NA, *et al*. The CD47-SIRPα signaling axis as an innate immune checkpoint in cancer. *Immunol Rev* 2017;276:145–64.
26 Soria G, Ben-Baruch A. The inflammatory chemokines CCL2 and CCL5 in breast cancer. *Cancer Lett* 2008;267:271–85.
27 Aldinucci D, Casagrande N. Inhibition of the CCL5/CCR5 axis against the progression of gastric cancer. *Int J Mol Sci* 2018;19:1477.
28 Zeng Z, Lan T, Wei Y, *et al*. CCL5/CCR5 axis in human diseases and related treatments. *Genes Dis* 2022;9:12–27.
29 Al Shihabi A, Davarifar A, Nguyen HTL, *et al*. Personalized chordoma organoids for drug discovery studies. *Sci Adv* 2022;8:eabl3674.
30 Scognamiglio G, De Chiara A, Parafioriti A, *et al*. Patient-derived organoids as a potential model to predict response to PD-1/PD-L1 checkpoint inhibitors. *Br J Cancer* 2019;121:979–82.
31 Sharifnia T, Wawer MJ, Chen T, *et al*. Small-molecule targeting of Brachyury transcription factor addiction in chordoma. *Nat Med* 2019;25:292–300.
32 Liu Z, Gao S, Zhu L, *et al*. Efficacy and safety of anlotinib in patients with unresectable or metastatic bone sarcoma: a retrospective multiple institution study. *Cancer Med* 2021;10:7593–600.
33 Lebellec L, Chauffert B, Blay J-Y, *et al*. Advanced chordoma treated by first-line molecular targeted therapies: outcomes and prognostic factors. A retrospective study of the french sarcoma group (GSF/GETO) and the association des neuro-oncologues d'expression française (ANOCEF). *Eur J Cancer* 2017;79:119–28.
34 Liu C, Jia Q, Wei H, *et al*. Apatinib in patients with advanced chordoma: a single-arm, single-centre, phase 2 study. *Lancet Oncol* 2020;21:1244–52.
35 Galon J, Angell HK, Bedognetti D, *et al*. The continuum of cancer immunosurveillance: prognostic, predictive, and mechanistic signatures. *Immunity* 2013;39:11–26.
36 Karpathiou G, Dridi M, Krebs-Drouot L, *et al*. Autophagic markers in chordomas: immunohistochemical analysis and comparison with the immune microenvironment of chordoma tissues. *Cancers (Basel)* 2021;13:2169.
37 Zou MX, Guo KM, Lv GH, *et al*. Clinicopathologic implications of CD8+/foxp3+ ratio and mir-574-3p/PD-L1 axis in spinal chordoma patients. *Cancer Immunol Immunother* 2018;67:209–24.
38 He G, Liu X, Pan X, *et al*. Cytotoxic T lymphocyte antigen-4 (CTLA-4) expression in chordoma and tumor-infiltrating lymphocytes (tils) predicts prognosis of spinal chordoma. *Clin Transl Oncol* 2020;22:2324–32.
39 Patel SS, Nota SP, Sabbatino F, *et al*. Defective HLA class I expression and patterns of lymphocyte infiltration in chordoma tumors. *Clin Orthop Relat Res* 2021;479:1373–82.
40 Duan W, Zhang B, Li X, *et al*. Single-cell transcriptome profiling reveals intra-tumoral heterogeneity in human chordomas. *Cancer Immunol Immunother* 2022;71:2185–95.
41 Lopez DC, Robbins YL, Kowalczyk JT, *et al*. Multi-spectral immunofluorescence evaluation of the myeloid, T cell, and natural killer cell tumor immune microenvironment in chordoma may guide immunotherapeutic strategies. *Front Oncol* 2022;12:1012058.
42 Aldinucci D, Borghese C, Casagrande N. The CCL5/CCR5 axis in cancer progression. *Cancers (Basel)* 2020;12:1765.
43 Wang S-W, Liu S-C, Sun H-L, *et al*. CCL5/CCR5 axis induces vascular endothelial growth factor-mediated tumor angiogenesis in human osteosarcoma microenvironment. *Carcinogenesis* 2015;36:104–14.
44 Ridley AJ, Schwartz MA, Burridge K, *et al*. Cell migration: integrating signals from front to back. *Science* 2003;302:1704–9.
45 Jiao X, Velasco-Velázquez MA, Wang M, *et al*. CCR5 governs DNA damage repair and breast cancer stem cell expansion. *Cancer Res* 2018;78:1657–71.
46 Cereijo R, Gavaldà-Navarro A, Cairó M, *et al*. CXCL14, a brown adipokine that mediates brown-fat-to-macrophage communication in thermogenic adaptation. *Cell Metab* 2018;28:750–63.
47 Stacchiotti S, Sommer J, Chordoma Global Consensus Group. Building a global consensus approach to chordoma: a position paper from the medical and patient community. *Lancet Oncol* 2015;16:e71–83.
48 Rinner B, Froehlich EV, Buerger K, *et al*. Establishment and detailed functional and molecular genetic characterisation of a novel sacral chordoma cell line, MUG-chor1. *Int J Oncol* 2012;40:443–51.
49 Bock C, Boutros M, Camp JG, *et al*. The organoid cell atlas. *Nat Biotechnol* 2021;39:13–7.